Peer-Reviewed Technical Communication

Space–Frequency Block Coding for Underwater Acoustic Communications

Eduard Valera Zorita and Milica Stojanovic, *Fellow, IEEE*

***Abstract*—In this paper, Alamouti space–frequency block coding, applied over the carriers of an orthogonal frequency-division multiplexing (OFDM) system, is considered for obtaining transmit diversity in an underwater acoustic channel. This technique relies on the assumptions that there is sufficient spatial diversity between the channels of the two transmitters, and that each channel changes slowly over the carriers, thus satisfying the basic Alamouti coherence requirement and allowing simple data detection. We propose an adaptive channel estimation method based on Doppler prediction and time smoothing, whose decision-directed operation allows for reduction in the pilot overhead. System performance is demonstrated using real data transmitted in the 10–15-kHz acoustic band from a vehicle moving at 0.5–2 m/s and received over a shallow-water channel, using quadrature phase-shift keying (QPSK) and a varying number of carriers ranging from 64 to 1024. Results demonstrate an average mean squared error gain of about 2 dB as compared to the single-transmitter case and an order of magnitude decrease in the bit error rate when the number of carriers is chosen optimally.**

***Index Terms*—Adaptive channel estimation, Alamouti, multiple-input–multiple-output (MIMO), orthogonal frequency-division multiplexing (OFDM), space–frequency block coding, underwater acoustic communication.**

I. Introduction

ORTHOGONAL frequency-division multiplexing (OFDM) is considered for frequency-selective underwater acoustic (UWA) channels as it offers low complexity of fast-Fourier-transform-based (FFT) signal processing, and ease of reconfiguration for use with different bandwidths. In addition, by virtue of having a narrowband signal on each carrier, OFDM is easily conducive to multiple-input–multiple-oputput (MIMO) system configurations.

OFDM–MIMO systems have been considered for UWA channels both for increasing the system throughput via spatial multiplexing [1], [2] and for improving the systems performance via spatial diversity [3]. A large body of work has also been devoted to single-carrier MIMO systems, addressing issues of space–time coding and iterative (turbo) equalization [4]–[7], frequency-domain processing [8], [9], Doppler compensation [10], and time-reversal methods [11] for spatial multiplexing.

The focus of our present work is on transmit diversity, which we pursue through the use of Alamouti coding applied across the carriers of an OFDM signal. Space–frequency block coding (SFBC) is chosen over traditional space–time block coding (STBC) as better suited for use with acoustic OFDM signals. Namely, while the Alamouti coherence assumption [12] may be challenged between two adjacent OFDM blocks on a time-varying acoustic channel [3], it is expected to hold between two adjacent OFDM carriers: Frequency coherence assumption coincides with the basic OFDM design principle which calls for the carriers to be spaced closely enough that the channel transfer function can be considered flat over each sub-band. Previous studies in radio communications have also revealed that space–frequency transmit diversity significantly outperforms space–time transmit diversity in fast fading environments when the normalized Doppler frequency is large [13], [14].

Two types of approaches have been considered for MIMO–OFDM acoustic systems: nonadaptive, where each block is processed independently using pilot-assisted channel estimation [1], and adaptive, where coherence between adjacent blocks is exploited via channel/Doppler tracking and prediction to enable decision-directed operation and reduce the pilot overhead [2]. Both approaches require front–end synchronization for initial Doppler compensation through signal resampling [15]. Front–end processing remains unchanged for multiple transmitters if they are colocated and experience the same gross Doppler effect. Otherwise, multiple resampling branches may be needed to compensate for transmitter-specific Doppler shifting [16].

Leveraging on the adaptive MIMO–OFDM design [2], we develop a receiver algorithm for the SFBC scenario. Specifically, we decouple the channel distortion into a slowly varying gain and a faster varying phase, which enables us to track these parameters at different speeds. For estimating the channel, we use either the orthogonal matching pursuit (OMP) algorithm [17] or a newly developed algorithm based on least squares with adaptive thresholding (LS–AT). This algorithm computes the full-size LS solution to the impulse response (IR) domain channel representation, then truncates it to keep only the significant IR coefficients. However, unlike the typical truncated LS solutions which use a fixed truncation threshold [2], the

Manuscript received August 17, 2012; revised December 30, 2013; accepted April 02, 2014. This work was supported in part by the U.S. Office of Naval Research (ONR) under Grants N00014-07-1-0738 and N00014-09-1-0700, and by the National Science Foundation (NSF) under Grant CNS-1212999.

Associate Editor: J. Gomes.

E. V. Zorita is with the Centre for Genomic Regulation, Barcelona 08003, Spain (e-mail: ezorita@mit.edu).

M. Stojanovic is with Northeastern University, Boston, MA 02115 USA (e-mail: millitsa@mit.edu).

Digital Object Identifier 10.1109/JOE.2014.2316558

threshold is determined adaptively so as to provide a proper level of sparseness. LS–AT is found to perform close to OMP, at a lower computational cost. Similar approaches have been proposed in the literature, where the threshold level is adaptively computed as a function of the noise variance in the time domain [18], [19]. Once an initial channel estimate is formed, its tracking continues via time smoothing. Simultaneously, an estimate of the residual Doppler scale is made for each of the two transmitters, and this estimate is used to predict and update the carrier phases in each new OFDM block.

The advantages of Alamouti SFBC are contingent upon frequency coherence, which increases as more carriers are packed within a given bandwidth (the bandwidth efficiency simultaneously increases). However, there is a fine line after which intercarrier interference (ICI) will be generated, and this line should not be crossed if simplicity of Alamouti detection is to be maintained. We assess this tradeoff through simulation and experimental data processing, showing the existence of an optimal number of carriers and an accompanying transmit diversity gain.

The paper is organized as follows. In Section II, we introduce the system model and discuss the channel assumptions. The receiver algorithm is described in Section III. In Section IV, results of simulation and experimental data processing are presented. Conclusion are summarized in Section V.

II. System Model

We consider a MIMO system with $M_T = 2$ transmitters and M_R receivers. OFDM is used with K subcarriers, equally spaced within the system bandwidth B at $\Delta f = B/K$. The OFDM symbol duration is $T = 1/\Delta f$, and a guard interval (cyclic prefix) of duration T_g, sufficient to accommodate the multipath spread T_{mp}, is added for the total block duration of $T' = T + T_g$. The symbols[1] are encoded using the Alamouti SFBC scheme, i.e., if k is the carrier *pair* index ($k = 0, \ldots, K/2-1$), during the nth OFDM block, the *simultaneously* transmitted symbols on carriers $2k$ and $2k+1$ are, respectively, $d_{2k}(n)$ and $d_{2k+1}(n)$ from the first transmitter, and $-d^*_{2k+1}(n)$ and $d^*_{2k}(n)$ from the second transmitter.

The channel transfer function observed on the carrier k' between transmitter t and receiver r during the nth OFDM block is denoted by $H^{t,r}_{k'}(n)$, $k' = 0, \ldots, K-1$. The received signal, corresponding to the kth coded carrier pair and the rth receiving element after FFT demodulation, is given by

$$\mathbf{y}^{rA}_{2k}(n) = \underbrace{\begin{bmatrix} H^{1,r}_{2k}(n) & H^{2,r}_{2k}(n) \\ -H^{2,r*}_{2k+1}(n) & H^{1,r*}_{2k+1}(n) \end{bmatrix}}_{\mathbf{C}^r_{2k}(n)} \mathbf{d}^A_{2k}(n) + \mathbf{z}^{rA}_{2k}(n) \tag{1}$$

[1]We use the term *data symbol* or just symbol to refer to the information modulated onto each carrier. A group of data symbols assigned to all carriers during one interval T is referred to as one OFDM symbol or one OFDM *block*. The corresponding time-domain waveform is also referred to as a block. Several successive blocks form one *frame*. Frames are separated by a synchronization preamble.

where

$$\mathbf{y}^{rA}_{2k}(n) = \begin{bmatrix} y^r_{2k}(n) \\ -y^{r*}_{2k+1}(n) \end{bmatrix}, \mathbf{d}^A_{2k}(n) = \begin{bmatrix} d_{2k}(n) \\ -d^*_{2k+1}(n) \end{bmatrix}$$

and

$$\mathbf{z}^{rA}_{2k} = \begin{bmatrix} z^r_{2k}(n) \\ -z^{r*}_{2k+1}(n) \end{bmatrix}$$

represents zero-mean additive noise components. If M_R receiving elements are used, their signals can be arranged into a single vector, so that the system is fully described by

$$\underbrace{\begin{bmatrix} \mathbf{y}^{1A}_{2k}(n) \\ \vdots \\ \mathbf{y}^{M_R A}_{2k}(n) \end{bmatrix}}_{\mathbf{y}^A_{2k}(n)} = \underbrace{\begin{bmatrix} \mathbf{C}^1_{2k}(n) \\ \vdots \\ \mathbf{C}^{M_R}_{2k}(n) \end{bmatrix}}_{\mathbf{C}_{2k}(n)} \mathbf{d}^A_{2k}(n) + \underbrace{\begin{bmatrix} \mathbf{z}^{1A}_{2k}(n) \\ \vdots \\ \mathbf{z}^{M_R A}_{2k}(n) \end{bmatrix}}_{\mathbf{z}^A_{2k}(n)}. \tag{2}$$

Based on this model, LS data estimates are obtained as

$$\hat{\mathbf{d}}^A_{2k}(n) = [\mathbf{C}^H_{2k}(n)\mathbf{C}_{2k}(n)]^{-1}\mathbf{C}^H_{2k}(n)\mathbf{y}^A_{2k}(n). \tag{3}$$

A. Alamouti Assumption

The Alamouti assumption, expressed for space–frequency coding, states that the channel does not change much over two consecutive carriers

$$H^{t,r}_{2k}(n) \approx H^{t,r}_{2k+1}(n). \tag{4}$$

When this assumption holds, the channel matrix satisfies the property

$$\mathbf{C}^{rH}_{2k}(n)\mathbf{C}^r_{2k}(n) = \underbrace{\left(|H^{1,r}_{2k}(n)|^2 + |H^{2,r}_{2k}(n)|^2\right)}_{E^r_{2k}(n)} \mathbf{I}_2 \tag{5}$$

where $\mathbf{I}_2$ is the 2×2 identity matrix. The LS data estimate (3) then reduces to

$$\hat{\mathbf{d}}^A_{2k}(n) = \frac{1}{\sum_r E^r_{2k}(n)} \mathbf{C}^H_{2k}(n)\mathbf{y}^A_{2k}(n). \tag{6}$$

Extraction of the transmit diversity gain through summation of individual channel's energies, and simplicity of data detection without matrix inversion, form the essence of Alamouti processing.

B. Channel Model

We model the UWA channel as

$$H^{t,r}_{k'}(n) = \sum_p h^{t,r}_p(n) e^{-\mathrm{j}2\pi f_{k'} \tau^{t,r}_p(n)} \tag{7}$$

where $h^{t,r}_p(n)$ and $\tau^{t,r}_p(n)$ represent, respectively, the gain and delay of the pth propagation path, and $f_{k'} = f_0 + k'\Delta f$ is the k'th carrier frequency. We further assume that the path gains

are slowly varying with the block index n, and that the delays are subject to compression/dilatation caused by motion at a constant relative velocity $v^{t,r}$ which does not change over a certain number of OFDM blocks. The delay is consequently modeled as

$$\tau_p^{t,r}(n) = \tau_p^{t,r}(n-1) - a^{t,r}T' = \tau_p^{t,r}(0) - a^{t,r}nT' \qquad (8)$$

where $a^{t,r} = v^{t,r}/c$ is the Doppler scaling factor. Our work specifically addresses the case in which both transmit and receive elements are colocated, and the major cause of motion is the motion of the transmitter. One can then assume that $a^{t,r} = a^t$ [2].

Synchronization at the receiver is performed independently for each receiving element. The receiver's reference time $\tau_0^r(0)$ is inferred from the composite received signal and set to 0. In general, however, one can have both $\tau_0^{1,r}(0) \neq 0$ and $\tau_0^{2,r}(0) \neq 0$, as the signals arriving from different transmitters may have traversed different distances. We note, however, that when the transmit elements are colocated and separated by only a few wavelengths $\lambda_0 = c/f_0$, the difference in the arrival times $\Delta\tau_0^r = |\tau_0^{1,r}(0) - \tau_0^{2,r}(0)|$ will be on the order of λ_0/c, e.g., a fraction of a millisecond for f_0 on the order of a few kilohertz. This delay difference (which is seen in the frequency domain as an additional linear phase component) is small enough that the resulting phase rotation of the transfer function $H_{k'}^{t,r}(n)$ will be slow over the carriers. The effect of delay difference will be further quantified through numerical examples in Section IV.

Given the delays (8), let us decompose the transfer functions (7) as follows:

$$H_{k'}^{t,r}(n) = A_{k'}^{t,r}(n)e^{\mathrm{j}\alpha_{k'}^t(n)} \qquad (9)$$

where

$$A_{k'}^{t,r}(n) = \sum_p h_p^{t,r}(n)e^{-\mathrm{j}2\pi f_{k'}\tau_p^{t,r}(0)} \qquad (10)$$

are the (complex-valued) gains, and

$$\alpha_{k'}^t(n) = 2\pi f_{k'}a^t nT' \qquad (11)$$

are the incremental phases of the two transmitters' channels. We note that the phases $2\pi f_{k'}\tau_p^{t,r}(0)$ are time invariant; hence, $A_{k'}^{t,r}(n)$ are only slowly varying as dictated by the path gains $h_p^{t,r}(n)$, while the dominant cause of time variation in $H_{k'}^{t,r}(n)$ are the phases $\alpha_{k'}^t(n)$. We will use these facts in Section III to design an adaptive channel tracking algorithm.

As far as the Alamouti assumption (4) is concerned, it will hold if

$$A_{2k+1}^{t,r}(n) \approx A_{2k}^{t,r}(n) \qquad \forall k,t,r \qquad (12)$$

and

$$e^{\mathrm{j}2\pi\Delta f a^t nT'} \approx 1 \qquad \forall t. \qquad (13)$$

In a properly designed OFDM system where $\Delta f \ll 1/T_{mp}$, the first set of assumptions (12) will hold provided that initial synchronization is sufficiently accurate with respect to each transmitter, such that $\Delta f\tau_0^{t,r}(0) \ll 1\ \forall t,r$, i.e., that neither channel exhibits significant phase rotation across the carriers. As mentioned earlier, this is a reasonable assumption for colocated transmitters. Regarding the second set of assumptions (13), they will hold as well since $\Delta fT' \sim 1$, and the residual Doppler factors a^t typically do not exceed 10^{-4} at the output of the digital resampler. Initial Doppler compensation is effectively achieved during the synchronization phase through signal resampling by a factor equal to the relative compression/dilation experienced by the received signal. The resampling factor is measured with the aid of synchronization probes inserted at both ends of each transmitted frame [15].

III. Receiver Algorithm

The key to successful data detection is channel estimation. We focus on a channel estimation method consisting of two steps: an initial step, which is based on pilots only, and subsequent adaptation, which involves data detection as well. The initial step constitutes conventional, one-shot (nonadaptive) estimation, and can also be used alone, i.e., it can be applied repeatedly throughout a frame of OFDM blocks without engaging adaptation (time smoothing).

Channel estimation is performed independently for each receiving element, and it is based on the Alamouti assumption. If the Alamouti assumption holds, the received signal can be represented as

$$\mathbf{y}_{2k}^r(n) = \mathbf{D}_{2k}(n)\underbrace{\begin{bmatrix} A_{2k}^{1,r}(n)e^{\mathrm{j}\alpha_{2k}^1(n)} \\ A_{2k}^{2,r}(n)e^{\mathrm{j}\alpha_{2k}^2(n)} \end{bmatrix}}_{\mathbf{H}_{2k}^r(n)} + \mathbf{z}_{2k}^r(n) \qquad (14)$$

where

$$\mathbf{D}_{2k}(n) = \begin{bmatrix} d_{2k}(n) & -d_{2k+1}^*(n) \\ d_{2k+1}(n) & d_{2k}^*(n) \end{bmatrix} = [\,\mathbf{d}_{2k}^1(n) \quad \mathbf{d}_{2k}^2(n)\,]$$

and

$$\mathbf{y}_{2k}^r(n) = \begin{bmatrix} y_{2k}^r(n) \\ y_{2k+1}^r(n) \end{bmatrix}, \quad \mathbf{z}_{2k}^r(n) = \begin{bmatrix} z_{2k}^r(n) \\ z_{2k+1}^r(n) \end{bmatrix}.$$

Assuming unit-amplitude PSK symbols, we have that

$$\frac{1}{2}\mathbf{D}_{2k}^H(n)\mathbf{D}_{2k}(n) = \mathbf{I}_2. \qquad (15)$$

Hence, if a particular pair of data symbols is known, the LS channel estimate is obtained directly from (14) as

$$\check{\mathbf{H}}_{2k}^r(n) = \frac{1}{2}\mathbf{D}_{2k}^H(n)\mathbf{y}_{2k}^r(n) \qquad (16)$$

i.e.,

$$\check{H}_{2k}^{t,r}(n) = \frac{1}{2}\mathbf{d}_{2k}^{tH}(n)\mathbf{y}_{2k}^r(n). \qquad (17)$$

A. One-Shot Channel Estimation

Pilot-based channel estimation exploits the discrete Fourier relationship between the channel coefficients in the transfer function (TF) domain and the IR domain, where there are typically many fewer nonzero coefficients. To estimate a channel with L nonzero IR coefficients, at least L pilots are needed for *each* transmitter. Considering a system with a typical multipath

spread of about 10 ms and a bandwidth of 5 kHz, the number of nonzero IR coefficients is on the order of 50. For simplicity, L is taken as a power of 2, and pilot *pairs* are inserted evenly, i.e., every K/L pairs of carriers.

TF coefficients of the pilot carriers are estimated using (16), and the inverse discrete Fourier transform (IDFT) is applied to obtain the IR coefficients[2]

$$\check{h}_m^{t,r}(n) = \frac{1}{L}\sum_{l=0}^{L-1} \check{H}_{lK/L}^{t,r}(n) e^{\mathrm{j}2\pi\frac{lm}{L}}, \qquad m = 0, \ldots, L-1 \tag{18}$$

or equivalently in matrix form

$$\check{\mathbf{h}}^{t,r}(n) = \frac{1}{L}\mathbf{F}_L^H \check{\mathbf{H}}^{t,r}(n) \tag{19}$$

where $\mathbf{F}_L$ is an appropriately defined DFT matrix.

1) Sparse Channel Estimation: In an acoustic channel, it is often the case that the vector of IR coefficients $\check{\mathbf{h}}^{t,r}(n)$ is sparse, with only $J < L$ significant coefficients. Methods for sparse channel estimation, and in particular the OMP algorithm, have been shown to be very effective in such situations [17], [20], [21]. These methods typically provide a sparse solution $\bar{\mathbf{h}}^{t,r}(n)$ that best matches the model $\check{\mathbf{H}}^{t,r}(n) = \mathbf{F}_L \bar{\mathbf{h}}^{t,r}(n)$ for a given input $\check{\mathbf{H}}^{t,r}(n)$ and a desired degree of sparseness J.

As an alternative to the OMP method, we consider a method of LS with adaptive thresholding. This method eliminates the need to set the desired degree of sparseness *a priori*, while keeping the computational load at a minimum. The LS–AT algorithm uses the design value T_{mp} as an upper bound of the multipath spread, and changes a truncation threshold γ until the *total* delay spread $\check{T}_{mp}$ of the sparse solution $\bar{\mathbf{h}}^{t,r}(n)$ fits into the design value. The threshold is initially set to $\gamma = 0.5$ of the strongest coefficient's magnitude. The IR coefficients whose relative magnitude is below the threshold are discarded, and if the resulting delay spread is found to be less than the design value T_{mp}, the threshold is lowered. Otherwise, it is increased. The algorithm proceeds in this manner for a predetermined minimum number of steps S. Thereafter, it continues if the threshold is to be raised further, and stops when a decreasing threshold is detected. The number of steps is chosen according to the desired resolution 2^{-S}. In the numerical analysis of Section IV, we employ 20 steps and T_{mp} equal to the guard interval. The algorithm is formalized in Algorithm 1.

Algorithm 1: Least Squares Adaptive Thresholding (LS–AT)

1: Define: S, T_{mp}
2: Initialize: $\gamma = 0.5$, *step* $= 1$, $\Delta\gamma = 0$
3: $\check{\mathbf{h}}^{t,r}(n) \leftarrow$ Compute channel IR given by (18)
4: **while** *step* $\le S$ **or** (*step* $> S$ **and** $\Delta\gamma > 0$) **do**
5: **for all** m **do**
6: $\bar{h}_m^{t,r}(n) = \begin{cases} \check{h}_m^{t,r}(n), & \text{if } |\check{h}_m^{t,r}(n)| > \gamma \max_m |\check{h}_m^{t,r}(n)| \\ 0, & \text{otherwise} \end{cases}$
7: **end for**
8: $\check{T}_{mp} \leftarrow$ Compute delay spread of $\bar{h}_m^{t,r}(n)$
9: **if** $T_{mp} \le \check{T}_{mp}$ **then**
10: $\Delta\gamma = 2^{-(step+1)}$
11: **else**
12: $\Delta\gamma = -2^{-(step+1)}$
13: **end if**
14: $\gamma \leftarrow \gamma + \Delta\gamma$
15: *step* $\leftarrow$ *step* $+1$
16: **end while**
17: **return** $\bar{\mathbf{h}}^{t,r}(n)$

The running estimate of the delay spread (line 8 of Algorithm 1) is computed as

$$\check{T}_{mp} = (L_{IR} - L_Z)T_s \tag{20}$$

where L_{IR} is the length of $\bar{\mathbf{h}}^{t,r}(n)$, L_Z is the maximum number of consecutive zeros found in the IR (considering its circularity), and T_s is the sampling period. If the guard time is chosen conservatively, a shorter T_{mp} can be used to reduce the effects of noise (occasional noise spikes that mistakenly become interpreted as channel taps). In the unlikely case that the actual delay spread exceeds T_{mp}, a serious penalty could result. Fortunately, this situation is easily detectable as it causes the algorithm to return exceptionally high values of the threshold, e.g., above 0.5. Should that occur, it would serve as an indication that T_{mp} needs to be increased and the procedure repeated.

Once the sparse IR $\bar{\mathbf{h}}^{t,r}(n)$ has been obtained, it is zero padded to the full length K, and the TF coefficients on all the carriers are estimated as the DFT of the so-obtained $1 \times K$ vector $\hat{\mathbf{h}}^{t,r}(n)$[3]

$$\hat{\mathbf{H}}^{t,r}(n) = \mathbf{F}_K \hat{\mathbf{h}}^{t,r}(n). \tag{21}$$

The TF coefficients are now used to form the channel matrices needed for data detection.

2) A Note on TF Coefficients and the $\Delta f/2$ Correction: The exact value of the initial observation for the first transmitter $\check{H}_{2k}^{1,r}(n)$, which is used as the input to the channel estimator, is obtained using (1) and (17) as

$$\begin{aligned} \check{H}_{2k}^{1,r}(n) &= \frac{1}{2}\mathbf{d}_{2k}^{1H}(n)\mathbf{y}_{2k}^r(n) = \frac{1}{2}\left[\, d_{2k}^*(n) \quad d_{2k+1}^*(n) \,\right] \\ &\quad \times \begin{bmatrix} H_{2k}^{1,r}(n)d_{2k}(n) - H_{2k}^{2,r}(n)d_{2k+1}^*(n) + z_{2k}^r(n) \\ H_{2k+1}^{1,r}(n)d_{2k+1}(n) + H_{2k+1}^{2,r}d_{2k}^*(n) + z_{2k+1}^r(n) \end{bmatrix} \\ &= \frac{1}{2}\left(H_{2k}^{1,r}(n) + H_{2k+1}^{1,r}(n)\right) \\ &\quad + \frac{1}{2}d_{2k+1}^*(n)d_{2k}^*(n)(H_{2k+1}^{2,r}(n) - H_{2k}^{2,r}(n)) \\ &\quad + \frac{1}{2}\left(d_{2k}^*(n)z_{2k}^r(n) + d_{2k+1}^*(n)z_{2k+1}^r(n)\right). \end{aligned} \tag{22}$$

[2]The IR coefficients are not to be confused with the path gains $h_p^{t,r}(n)$.

[3]Because the sparse IR has been obtained by removing samples from $\check{\mathbf{h}}^{t,r}(n)$, the resulting transfer function may contain distortion at the ends of the spectrum. To avoid this effect, null carriers can be added at the end of the LS estimates (17) and removed from $\hat{\mathbf{H}}^{t,r}$ after sparsing the IR.

A similar relationship holds for the other transmitter. Considering the fact that $H^{2,r}_{2k+1}(n) \approx H^{2,r}_{2k}(n)$, and that the input noise is zero mean, we have that

$$E\left\{\breve{H}^{1,r}_{2k}(n)\right\} = \frac{H^{1,r}_{2k}(n) + H^{1,r}_{2k+1}(n)}{2} \approx H^{1,r}_{2k+\frac{1}{2}}(n). \quad (23)$$

Hence, channel estimation will effectively yield a TF coefficient that lies midway between the carriers $2k$ and $2k+1$, and this fact can be exploited to refine the final estimate. To do so, one can compute the DFT (21) at twice the resolution, then select every other element of the so-obtained TF vector, starting with a delay of one. Equivalently, one can compute (21) using the original resolution (K-point FFT) but with an input vector $\hat{\mathbf{h}}^{t,r}(n) = [\hat{h}^{t,r}_l(n)]^{K-1}_{l=0}$ replaced by $\hat{\mathbf{h}}^{t,r}_{1/2}(n) = [\hat{h}^{t,r}_l(n)e^{-\mathrm{j}\pi l/K}]^{K-1}_{l=0}$.

3) Data Detection: Channel matrix $\hat{\mathbf{C}}_{2k}(n)$ is now filled with the TF estimates $\hat{H}^{t,r}_{k'}(n)$ according to the pattern (1) and (2), and the data symbols are estimated according to (6) as

$$\hat{\mathbf{d}}^A_{2k}(n) = \frac{1}{\mathrm{tr}\left[\hat{\mathbf{C}}^H_{2k}(n)\hat{\mathbf{C}}_{2k}(n)\right]}\hat{\mathbf{C}}^H_{2k}(n)\mathbf{y}^A_{2k}(n). \quad (24)$$

These estimates are fed to the decoder if additional channel coding is used, or used directly to make hard decisions. In either case, the process of decision making is denoted as

$$\tilde{\mathbf{d}}^A_{2k}(n) = \mathrm{dec}\left[\hat{\mathbf{d}}^A_{2k}(n)\right]. \quad (25)$$

B. Adaptive Channel Estimation

The goal of adaptive channel estimation is to exploit the time correlation present in the channel so as to reduce the pilot overhead. To do so, we draw on the earlier channel decomposition into the slowly varying gains $A^{t,r}_{k'}(n)$, and phases $\alpha^t_{k'}(n)$, whose variation in time is dictated by (possibly slowly varying) Doppler factors $a^t(n)$. We target these sets of parameters individually to accomplish effective channel tracking. The adaptive algorithm proceeds in several steps, carried out for each block n.

1) Decision Making: Let us assume that predictions $\tilde{A}^{t,r}_{k'}(n)$ and $\tilde{\alpha}^t_{k'}(n)$, made at the end of a previous block from the estimates $\hat{A}^{t,r}_{k'}(n-1)$ and $\hat{\alpha}^t_{k'}(n-1)$, are available at the beginning of the current block n. These predictions are used to form the channel matrices $\tilde{\mathbf{C}}_{2k}(n), k = 0, \ldots, K/2-1$, which are in turn used to make symbol decisions

$$\tilde{\mathbf{d}}^A_{2k}(n) = \mathrm{dec}\left[\frac{1}{\mathrm{tr}\left[\tilde{\mathbf{C}}^H_{2k}(n)\tilde{\mathbf{C}}_{2k}(n)\right]}\tilde{\mathbf{C}}^H_{2k}(n)\mathbf{y}^A_{2k}(n)\right]. \quad (26)$$

The symbol decisions are now treated as pilots, of which there may be as many as $L = K$, and they are used to update the phases and the channel estimates.

2) Sparse Channel Estimation: Let us denote the chosen channel estimation algorithm, be it OMP, LS–AT or similar, by $\mathcal{CE}(\cdot)$. This algorithm is applied to obtain the one-shot K-point channel estimate

$$\hat{\mathbf{H}}^{t,r}(n) = \mathcal{CE}\left(\left\{\tilde{\mathbf{d}}^{tH}_{2k}\mathbf{y}^r_{2k}(n)\right\}^{K/2-1}_{k=0}\right). \quad (27)$$

3) Phase Tracking: To update the phases, we measure the phase diferencies [angle $\angle(\cdot)$] between the estimates made for the current block (27) and the outdated estimates from the previous block

$$\Delta\alpha^t_{k'}(n) = \angle\sum_{r=1}^{M_R}\frac{\hat{H}^{t,r}_{k'}(n)}{\tilde{A}^{t,r}_{k'}(n)e^{j\hat{\alpha}^t_{k'}(n-1)}}. \quad (28)$$

The phase difference is thus obtained, and the Doppler factors for the current block are now estimated as

$$\hat{a}^t(n) = \frac{1}{K}\sum_{k'=0}^{K-1}\frac{\Delta\alpha^t_{k'}(n)}{2\pi f_{k'}T'}. \quad (29)$$

The phases are finally updated as

$$\hat{\alpha}^t_{k'}(n) = \hat{\alpha}^t_{k'}(n-1) + 2\pi\hat{a}^t(n)f_{k'}T'. \quad (30)$$

4) Channel Tracking: The updated $\hat{\alpha}^t_{k'}(n)$ are now used to compensate for the time-varying phase of $\hat{H}^{t,r}_{k'}(n)$, and the channel gains are updated as

$$\hat{A}^{t,r}_{k'}(n) = \lambda\hat{A}^{t,r}_{k'}(n-1) + (1-\lambda)\hat{H}^{t,r}_{k'}(n)e^{-\mathrm{j}\hat{\alpha}^t_{k'}(n)} \quad (31)$$

where $\lambda \in [0,1]$.

5) Refining the Symbol Decisions: At this point, one can repeat data detection using the updated estimates. However, this step may not be necessary, as the entire system operation is contingent upon the assumption that the channel varies slowly enough that the gain/phase prediction is accurate.

6) Predictions for the Next Block: Finally, predictions are made for the next block. The gain is predicted simply as

$$\tilde{A}^{t,r}_{k'}(n+1) = \hat{A}^{t,r}_{k'}(n) \quad (32)$$

while the phase predictions are made as

$$\tilde{\alpha}^t_{k'}(n+1) = \hat{\alpha}^t_{k'}(n) + 2\pi f_{k'}\hat{a}^t(n)T'. \quad (33)$$

The gain and phase predictions (32) and (33) will be used in the next iteration to form the channel matrices $\tilde{\mathbf{C}}_{2k}(n+1)$ required to compute (26).

Initialization: The phases and the Doppler factors are initially set to zero: $\hat{\alpha}^t_{k'}(0) = 0$ and $\hat{a}^t(0) = 0$. The algorithm starts by estimating the channel during the block $n = 0$, which yields the TF coefficients $\hat{A}^{t,r}_{k'}(0)$. Full operation starts at $n = 1$ with predictions $\tilde{A}^{t,r}_{k'}(1) = \hat{A}^{t,r}_{k'}(0)$, and $\tilde{\alpha}^t_{k'}(1) = 0$.

IV. Results

The performance of the SFBC–OFDM system was tested using synthetic data (simulation) as well as real data collected during the June 2010 Mobile MIMO Acoustic Communications Experiment (MACE10). The test channel used for simulation

Fig. 1. Experiment location. The experiment was conducted at 60 mi southwest of Martha's Vineyard island.

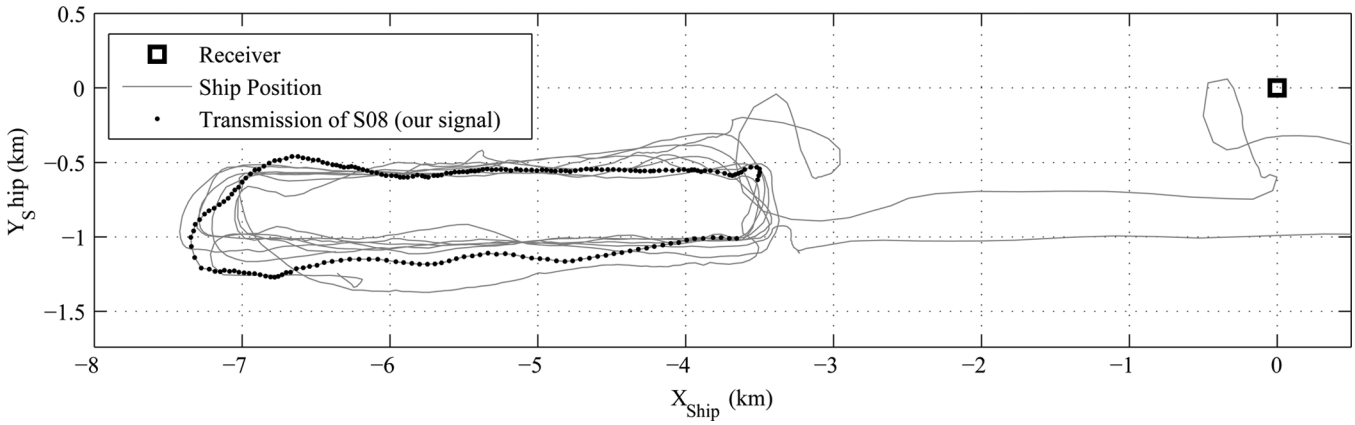

Fig. 2. Ship trajectory. Signals were transmitted from two colocated transmitters moving at 0.5–2 m/s along the indicated loop and recorded at a fixed vertical array located at coordinates (0, 0).

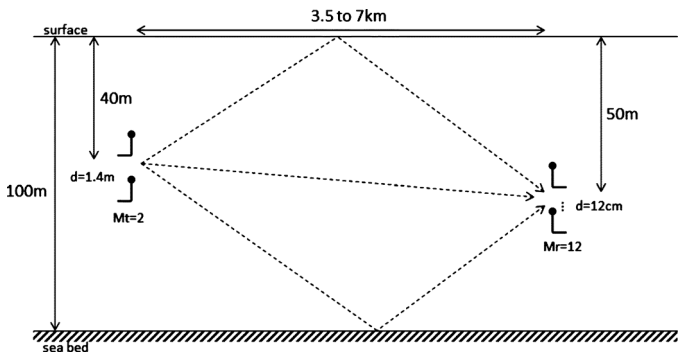

Fig. 3. Experiment geometry.

was constructed to reflect the experimental conditions, which are described below.

TABLE I
MACE EXPERIMENT SIGNAL PARAMETERS

Bandwidth, B	4883 Hz
First carrier frequency, f_0	10 580 Hz
Sampling frequency, f_s	39 062 Hz
Number of carriers, K	64, 128, 256, 512, 1024
Carrier spacing, Δf [Hz]	76, 38, 19, 10, 5
OFDM Block duration, T [ms]	13, 26, 52, 104, 210
Guard interval, Tg	16 ms
Symbols per frame, N_d	8192 QPSK
Blocks per frame, N	128, 64, 32, 16, 8
Bitrate, R [kbps]	4.3, 5.9, 7.2, 8.1, 8.7
Channel code	Hamming (14,9)

A. Experiment Description

The experiment was conducted by the Woods Hole Oceanographic Institution (WHOI, Woods Hole, MA, USA) at a location 60 mi south of Martha's Vineyard island (see Fig. 1). During the experiment, the transmitter array was deployed from a vessel moving in a repeated circular pattern, toward and away from the receiver, as shown in Fig. 2. The geometry of the experimental channel is shown in Fig. 3.

The experiment lasted for seven days, and the Alamouti SFBC signals were transmitted in the 10–15-kHz acoustic band in limited intervals during days 5, 6, and 7. Table I summarizes the signal parameters used in the experiment. QPSK modulation was used on all carriers, whose number ranged from 64 to 1024. Transmission was organized in frames, each containing 8192 data symbols divided into a varying number of OFDM blocks. The blocks were separated by a guard interval of 16 ms, and a synchronization probe was inserted at each end of a frame. With adaptive processing, pilot symbols were used only in the first block. The resulting overhead is 0.78% (with $K = 64$), 1.56% (with $K = 128$), and 3.13% (with $K = 256, 512, 1024$).

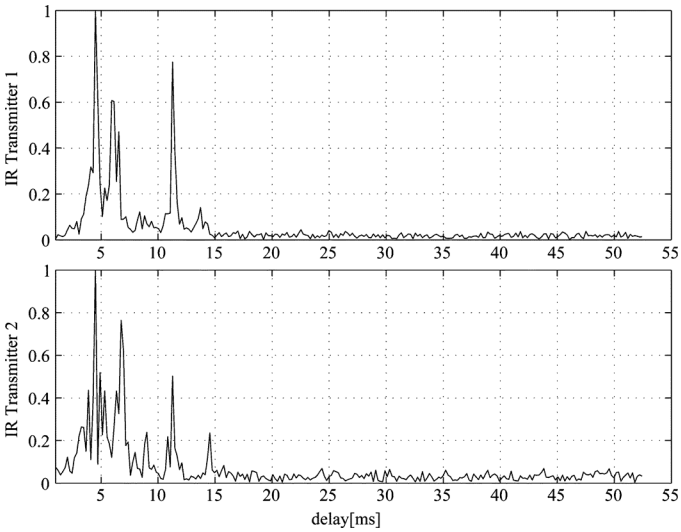

Fig. 4. Snapshots of channel response observed between the Alamouti pair of transmitters and a common receiver.

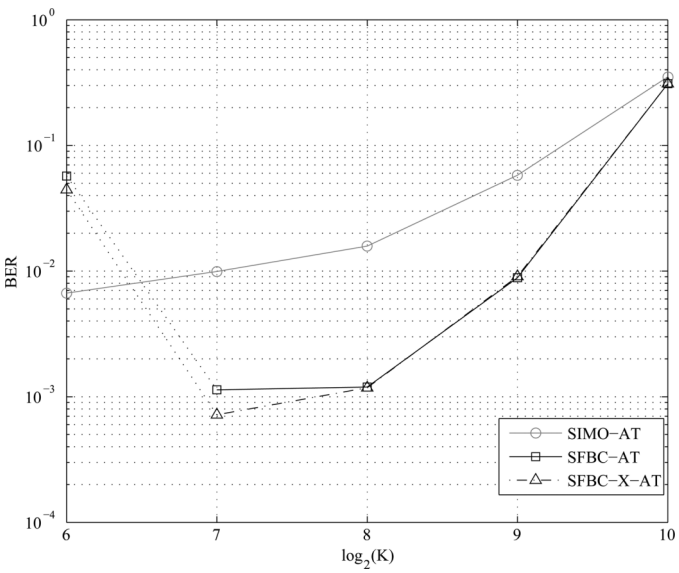

Fig. 5. Simulation: BER versus number of carriers. SNR = 15 dB, $M_R = 2$ receiving elements, and channel Doppler spread $B_d = 1$ Hz. Label X indicates full channel inversion (3).

With nonadaptive processing (block-by-block independent detection), the required overhead is 50% ($K = 512$) and 25% ($K = 1024$).[4]

Fig. 4 shows a snapshot of the channel IR (magnitude) obtained directly from the LS estimates. The channel has a sparse structure, and several of the multipath arrivals are well resolved. The total delay spread is about 12 ms in this case. Throughout the experiment, however, the multipath spread varied between 5 and 16 ms.

B. Simulation Results

The simulation test channel is generated according to (7) and (8), where the path gains $h_p^{t,r}$ and delays $\tau_p^{t,r}(0)$ are initialized using a library of the actual channels from the MACE10 experiment. Random variation is added to these path gains using a Ricean model, which was found to provide a good match for this type of channel [22]. Specifically, the Rice $\mathcal{K}$ factors are set to $\mathcal{K}_1 = 5$ for the direct path, $\mathcal{K}_2 = 0.5$ for the bottom-reflected path, and $\mathcal{K}_3 = 0$ for surface reflections. The random variation follows an AR-1 process with exponentially decaying time correlation and Doppler spread B_d.

The arrival time difference (recall the discussion of Section II-B) is set to $\Delta\tau_0^r = 0.3$ ms for all receiving elements, and the Doppler factors experience a linear increase from 0 at the beginning of a frame to 4×10^{-4} at the end of a frame.

Fig. 5 illustrates the bit error rate (BER) as a function of the number of carriers in an adaptive Alamouti SFBC–OFDM system.[5] As a benchmark, we use a single-input–multiple-output (SIMO) system implemented with the same channel estimator as the MIMO system and maximal-ratio combining (MRC). The SIMO and MIMO systems operate using the same total transmit power. The MIMO system performance is also shown in a configuration with full channel inversion (3), labeled SFBC-X. Each point is a result of averaging over all carriers and 300 frames, each generated using independent noise and fading realizations.

The SFBC system achieves the best performance with 128 and 256 carriers. With more carriers, performance degrades because of the gradual loss of time coherence and the rise of ICI. With fewer carriers ($K = 128$ in this example), there is a gradual loss of frequency coherence, which may eventually start to violate the Alamouti assumption (4). SFBC-X thus gains a slight advantage at $K = 128$. The very poor performance at $K = 64$ is an artifact of having insufficiently many pilots to perform channel estimation—at most $K/2 = 32$ pilots are available per transmitter, sufficing to cover only $32/B = 6.4$ ms of multipath, while the true multipath spread is about twice as long. (An actual system would not be designed in this manner; the $K = 64$ MIMO point is included only for the sake of illustration.) The rest of the values represent system configurations in which the tradeoff between frequency coherence and time coherence is well resolved.

In Fig. 6, we investigate the effect of synchronization mismatch, i.e., receiver's sensitivity to the difference in the times of signal arrival from the two transmitters. The figure shows the mean squared error (MSE) versus the delay difference, which is taken to be equal for all the receiving elements, $\Delta\tau_0^r = \Delta\tau_0$. As we conjectured in Section II-B, the system can tolerate delay differences that do not produce significant TF phase rotation across carriers, and the result of Fig. 6 confirms the fact that the performance remains unaltered for delays up to a millisecond. The difference in delay of 1 ms corresponds to the travel length difference of 1.5 m, which accidentally almost coincides with the transmit element spacing used in the MACE10 experiment. This distance in turn corresponds to ten wavelengths $\lambda_0 = c/f_0 = 0.15$ m, a separation that is sufficiently large to achieve spatial diversity.

In Fig. 7, we investigate the system performance as a function of the signal-to-noise ratio (SNR), defined as the usual E_b/N_0 value. Imperfect channel estimation due to Doppler spread ($B_d = 1$ Hz) is the cause of the observable error floor. A

[4]A 100% overhead would be needed with $K = 256$ or less.

[5]Unless stated otherwise, raw (uncoded) BER is shown.

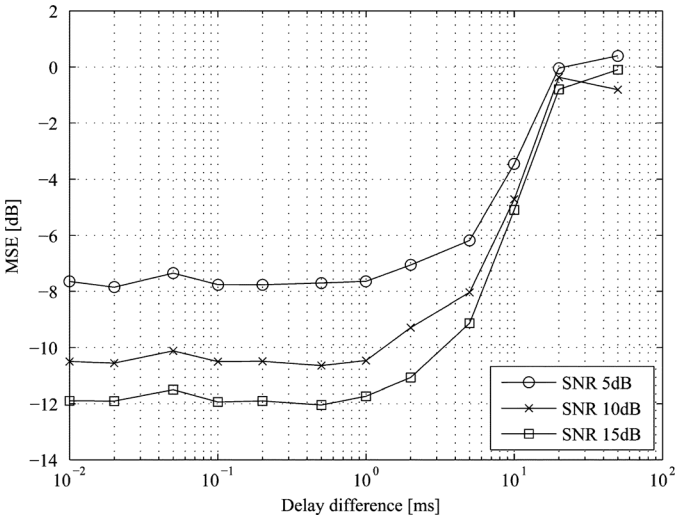

Fig. 6. Performance sensitivity to synchronization mismatch between transmitters: MSE versus delay difference $\Delta\tau_0(0)$. $K = 256$ carriers and $M_R = 6$ receiving elements.

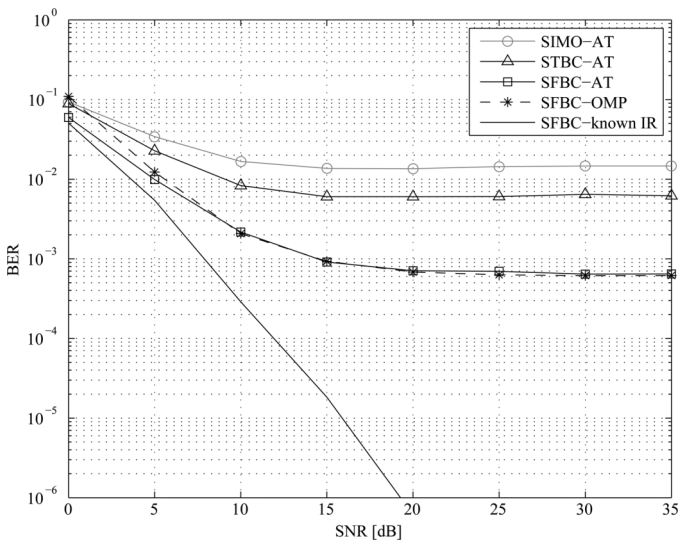

Fig. 7. Performance comparison between SIMO, STBC, and SFBC with different channel estimation algorithms: LS–AT and OMP. $K = 256$, $M_R = 2$ receivers, and $B_d = 1$ Hz.

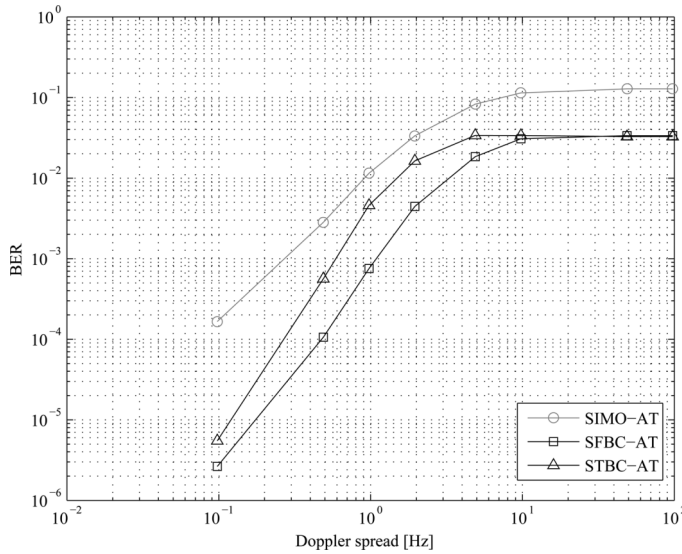

Fig. 8. Performance comparison between SIMO, STBC, and SFBC for different channel variation rates. SNR = 20 dB, $K = 256$, and $M_R = 2$ receivers.

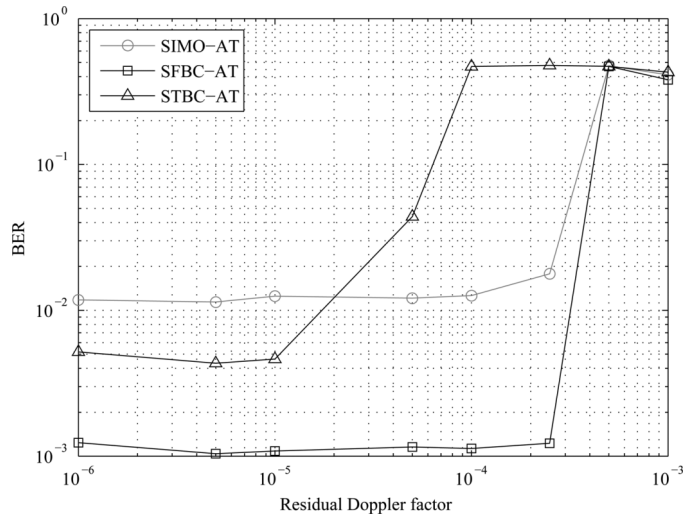

Fig. 9. Performance comparison between SIMO, STBC, and SFBC for different residual relative velocities. SNR = 15 dB, $K = 256$, and $M_R = 2$ receivers, $B_d = 1$ Hz.

known-IR curve is provided as a reference. STBC refers to the space–time implementation of the Alamouti code, as proposed in [3]. The SFBC system outperforms SIMO and STBC in terms of BER by a factor of 20 and 9, respectively. The system that uses LS with adaptive thresholding for channel estimation, as described in Section III-A, is labeled as AT, and is compared with channel estimation based on OMP. We note that the two algorithms have almost identical performance. LS–AT offers lower computational complexity, and may thus be preferred. The performance and computational cost of various algorithms will be discussed in more detail in Section IV-C.

System performance in different channel dynamics, i.e., at different values of the Doppler spread B_d, is illustrated in Fig. 8. The gain achieved with SFBC is approximately constant with respect to the SIMO case, provided that both perform channel estimation every block. However, the STBC system requires longer channel coherence time, and this fact translates to a limited gain and earlier saturation.

Finally, in Fig. 9, we investigate the system performance as a function of the residual Doppler factor introduced in Section II-B. This result clearly demonstrates the advantages of SFBC over STBC on a time-varying channel. While coding in time requires the channel to remain constant over two adjacent blocks, coding in frequency requires it to stay constant only over one block. As a result, SFBC tolerates higher residual Doppler scales than does STBC (the breakaway point at which the BER rapidly increases occurs later for SFBC). A second type of advantage is also evident: As residual Doppler scaling vanished, SFBC maintains better performance. This behavior is attributed to better handling of the inherent channel variation present in the Ricean-distributed path gains (described in Fig. 8).

C. Experimental Results

Experimental data available for our study included 87 transmissions performed once every 4 min. Each transmission in-

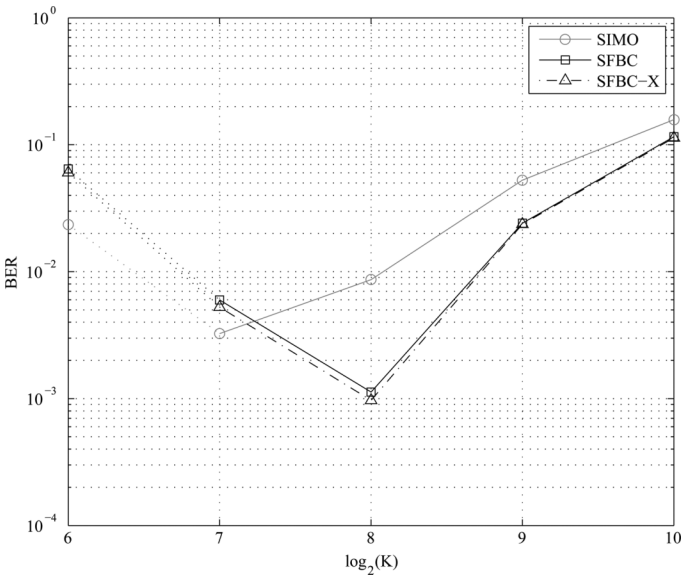

Fig. 10. Experiment: BER (uncoded) versus the number of carriers. $M_R = 12$ receiving elements. Each point represents an average over all carriers and frames.

cluded one frame of OFDM blocks with 64 carriers, one frame with 128 carriers, etc. During the time when these signals were transmitted, the source moved at a varying speed, ranging from 0.5 to 2 m/s. The results of real data processing are presented in terms of BER and MSE averaged over all the blocks and all the carriers, similarly as with simulation.[6] The LS–AT algorithm was used for channel estimation in the experimental results.

Fig. 10 shows the BER as a function of the number of carriers. We observe a similar trend as with synthetic data (Fig. 5), with the best performance at $K = 256$, corresponding to the carrier spacing $\Delta f = 19$ Hz. SFBC and SIMO are again compared fairly, as the same transmit power was used for both types of signals. Shown also is the method that uses full matrix inversion for LS data detection (SFBC-X) defined in (3), demonstrating that simple Alamouti detection incurs only a small penalty when the spacing between carriers is sufficiently large to violate the channel coherence assumption (12), i.e., for values of K below 256. The Alamouti assumption is better justified with more carriers, while the bandwidth efficiency is simultaneously increased. The MSE gain with respect to the SIMO case remains approximately constant for $K \geq 256$, on the order of 2 dB. At $K = 64$ and $K = 128$, there is a gradual loss of frequency coherence, and a sufficient number of observations is not provided to cover the multipath spread in all situations.

Fig. 11 shows the MSE evolution in time observed during several hours of one day of the experiment. SFBC outperforms SIMO–MRC uniformly, by about 2 dB over the 51 consecutive frames. Predicting the MIMO performance gain for a practical system remains difficult due to the unknown channel statistics. However, analytical results are available for coded OFDM systems operating over channels with specific distortion and known fading distribution [14], [23]–[25]. SFBC–ECC refers to the

[6]Those frames in which front–end synchronization failed were not included in the statistics.

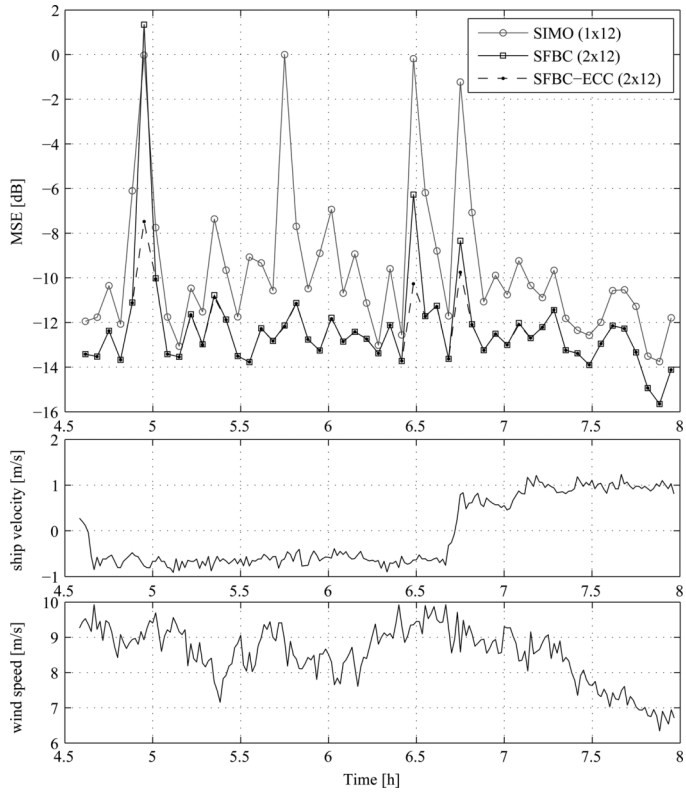

Fig. 11. MACE experiment, day 5: MSE evolution in time. $K = 256$ and $M_R = 12$ receiving elements.

case in which error correction coding (ECC) is exploited by the receiver to improve the reliability of decisions used for adaptive channel estimation.[7] Coding reduces the occasional MSE excursions (around hours 5 and 6.5) and effectively keeps the MSE below -7 dB throughout all the blocks. Comparing the MSE performance to the wind speed reveals an interesting correlation. The MSE is higher during the first three hours while the wind is stronger, and decreases at the end as the wind slows down. The MSE also behaves less erratically during the calmer wind period. Incidentally, this last period is accompanied by an increased transmitter velocity, which does not affect the performance. The largest excursions of the MSE are observed at hours 5 and 6.5 when the wind speed reaches highest values. Increased surface activity during those periods is believed to cause faster fading on the scattered paths, causing loss in performance of signal processing.

Fig. 12 shows the sensitivity to synchronization mismatch. For this measurement, signals from different transmitters were sent in successive nonoverlapping time intervals, so that they could be synchronized separately and combined after adding an artificial delay. Similarly as with synthetic data (Fig. 6), we observe that the performance remains unaffected for delay differences up to about 1 ms. While the delay difference in the current system geometry with colocated transmitters is within this limit, we note that additional synchronization techniques become necessary for cooperative transmission scenarios with spatially distributed transmitters.

[7]ECC is used here only to refine the channel estimates, which are then used to estimate the data symbols in the same manner as for the uncoded case. Compared to the uncoded system, the throughput is reduced by 35%.

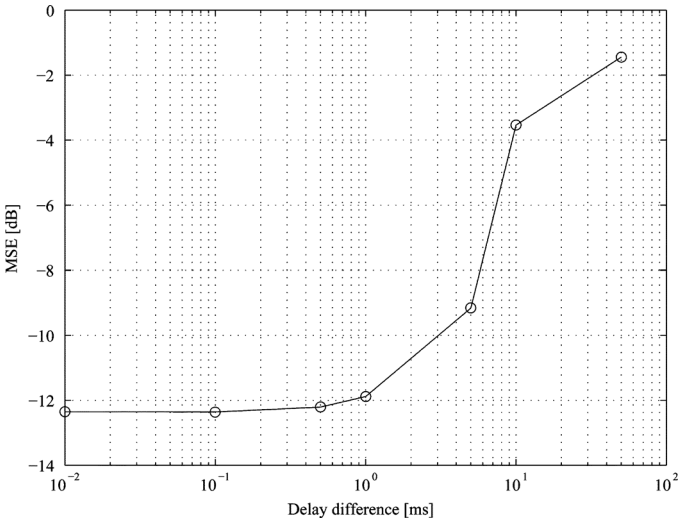

Fig. 12. Performance sensitivity to synchronization mismatch between transmitters: MSE versus delay difference $\Delta\tau_0(0)$. MACE10 data with $K = 256$ carriers and $M_R = 12$ receiving elements.

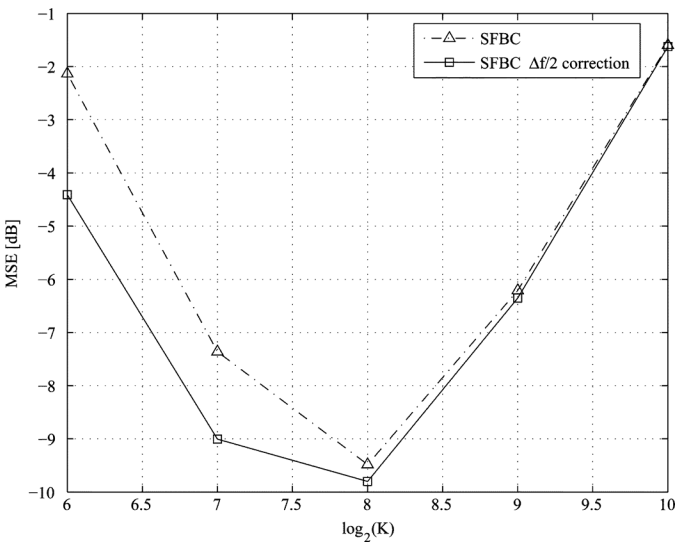

Fig. 13. System performance with and without the $\Delta f/2$ correction. Results are shown for a single MACE10 frame. $M_R = 12$ receiving elements.

1) The $\Delta f/2$ Correction: In Fig. 13, we investigate the benefits of additional processing applied to the TF coefficient estimates to correct for the $\Delta f/2$ offset (Section III-A2). This result shows that the $\Delta f/2$ correction provides a gain when the number of carriers is below the optimum, i.e., when there is a loss of frequency coherence due to the increased carrier separation. The gain is about 2 dB for $K = 64$ and 128, 0.5 dB for $K = 256$, and negligible thereafter.

2) Comparison of Sparse Channel Estimation Methods: Finally, we take a closer look at the performance of several channel estimation algorithms, namely LS–AT, LS with a fixed truncation threshold γ, and OMP. Fig. 14 shows the performance of LS–AT and LS with a fixed threshold. Clearly, adaptive thresholding outperforms fixed thresholding, and in fact represents a bound on its performance. The optimal threshold for a given *physical* channel depends on the number of carriers. Specifically, it decreases with K, as more observations are available for the channel estimator, and, hence, the quality of the estimate improves *vis-à-vis* noise.

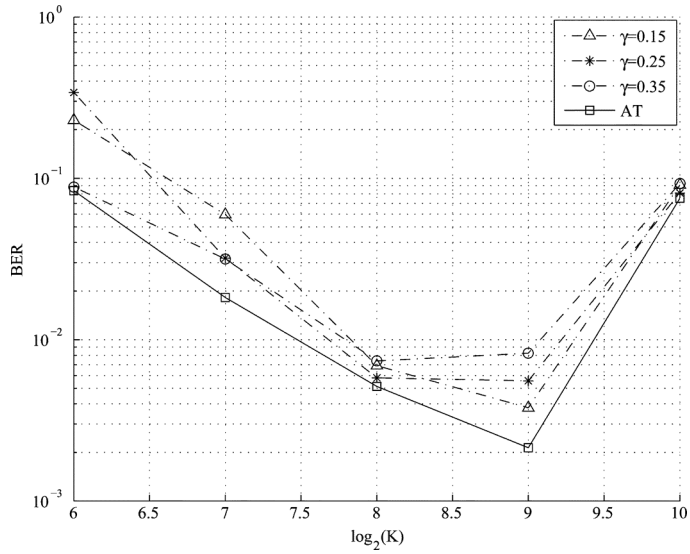

Fig. 14. Comparison between adaptive-threshold (20 steps) and fixed-threshold methods; single MACE10 frame. $M_R = 12$ receiving elements.

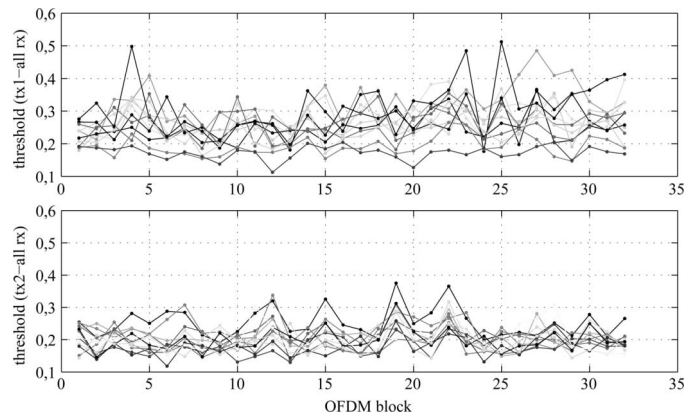

Fig. 15. Adaptive threshold values for different TX/RX pairs during transmission of one MACE10 frame. $M_R = 12$ receiving elements and $K = 256$ carriers.

To illustrate the performance of adaptive thresholding, we show in Fig. 15 several thresholds found by LS–AT, where each curve represents the evolution of the threshold used to estimate each transmitter–receiver channel within an entire frame (32 OFDM blocks for $K = 256$). Most threshold levels lie in the region between 0.15 and 0.30, but they may change as much as 0.30 from one OFDM block to another. The main reason for the erratic evolution is the formation of noise peaks away from the useful IR. These peaks appear randomly and cause the algorithm to occasionally raise the threshold. This observation speaks strongly in favor of adaptive threshold setting.

Fig. 16 shows the comparison between LS–AT, the OMP algorithm, and the ICI-ignorant algorithm proposed in [20]. The latter derives the channel directly from the received signal using a dictionary, which is generated with the transmitted pilots, and has a small loss in performance mainly because it treats the transmitted data as independent. The OMP algorithm solves the model $\check{\mathbf{H}}^{t,r}(n) = \mathbf{F}_L \bar{\mathbf{h}}^{t,r}(n)$ using a stopping criterion that measures the relative energy contribution of the last tap obtained. When this energy exceeds a predefined threshold (specified in decibels relative to the total energy) the algorithm stops and the last tap is discarded [21]. This criterion provides certain

TABLE II
COMPUTATIONAL COMPLEXITY OF SPARSE CHANNEL ESTIMATION ALGORITHMS FOR AN OFDM SYSTEM WITH K CARRIERS

		LS fixed threshold	LS-AT ($\mathcal{S} = 20$ steps)	OMP (-23dB)
number of operations for	initialization	$K^2 + 2K$	$K^2 + K$	$2K^2 + K$
	i-th iteration	-	$3K$	$i^2 + 2iK + K$
average (max) number of iterations	K=256	-	20.96 (31)	84.45 (119)
	K=512	-	20.89 (29)	68.20 (111)

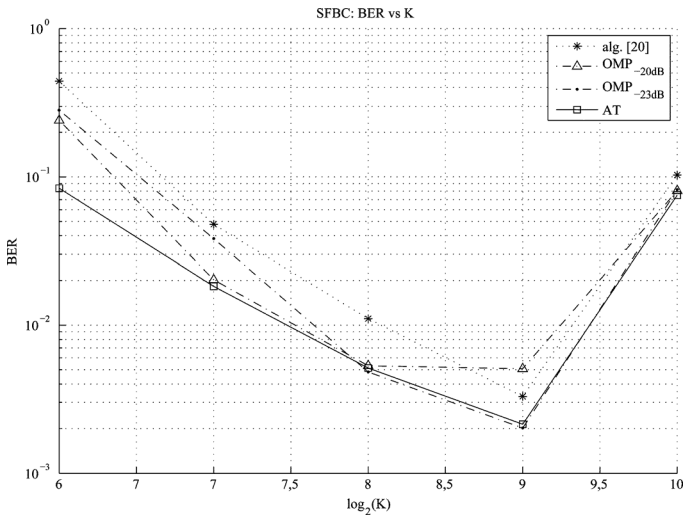

Fig. 16. Comparison between adaptive threshold (20 steps), OMP, and algorithm in [20]; single MACE10 frame. $M_R = 12$ receiving elements.

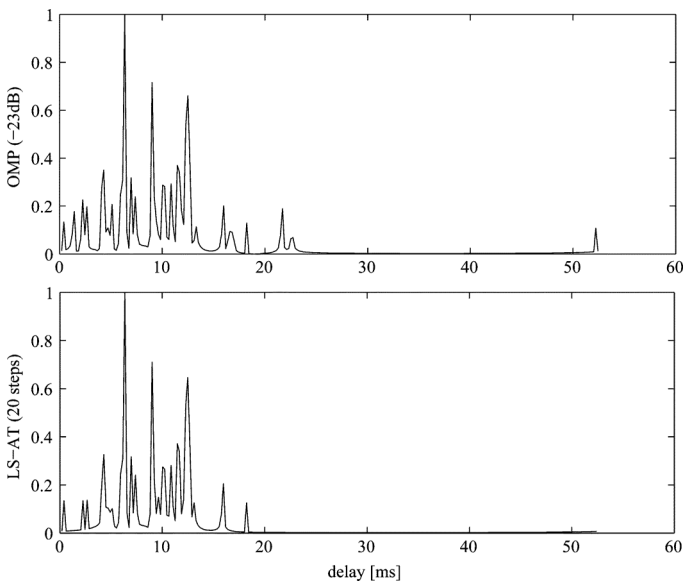

Fig. 17. Example of channel responses (magnitude) estimated by the OMP and LS–AT algorithms.

adaptability to the channel; however, the threshold has to be defined in terms of the expected noise and multipath intensity profile. As a result, OMP achieves the performance of LS–AT only in certain regions of K (different for each threshold). Fig. 17 shows an example of channel responses estimated by LS–AT and OMP algorithms.

The computational costs of fixed thresholding, adaptive thresholding, and OMP are compared in Table II. The table lists the number of operations and the average and the maximum number of iterations required to estimate each IR. Each estimated IR of length $K = 256$ required an average of 2.2×10^6 operations for the OMP algorithm, while LS–AT executed 8×10^4 operations, i.e., it was 20–30 times faster while offering comparable performance. The LS–AT algorithm effectively reduces the number of iterations by virtue of its convergence in the time domain, whereas the OMP algorithm requires an iteration for each estimated tap. Since it only requires a K size comparison and less-than-$2K$ size subtraction per iteration, LS–AT is well conducive to a digital signal processor (DSP) implementation.

V. CONCLUSION

MIMO spatial diversity was investigated for underwater acoustic communications through the use of Alamouti space–frequency coding coupled with OFDM. The use of space–frequency coding, as opposed to space–time coding, is motivated by the fact that frequency coherence naturally exists between the carriers of a properly designed (ICI-free) OFDM system. While it is needed to support FFT-based OFDM channel equalization, frequency coherence simultaneously supports Alamouti detection, which accomplishes MIMO crosstalk elimination without the need for matrix inversion.

Space–frequency-coded OFDM can be used both in a non-adaptive framework where the receiver detects each block of K carriers independently, or in an adaptive framework where the receiver exploits the knowledge of a physical propagation model to track those channel parameters that are varying slowly in time. We proposed a sparse channel identification algorithm based on LS–AT, and found that this algorithm operates close to OMP, at a lower computational complexity. For the adaptive setting, we proposed an algorithm that targets 1) the Doppler scaling factors corresponding to the two transmitters of the Alamouti pair; and 2) the respective channel gains that remain slowly varying once the Doppler shifts have been removed. More specifically, adaptive channel estimation targets the slowly varying, sparse IR coefficients, and employs further time smoothing across the OFDM blocks. Channel tracking is enabled by block-adaptive phase correction, which relies on estimating the Doppler scaling factors to predict each carrier's phase for the next OFDM block.

System performance was illustrated through simulation and with real data recorded in a mobile acoustic channel. Experimental results demonstrate the feasibility of space–frequency-coded OFDM, with a uniform 2-dB gain over the SIMO benchmark. The gain is contingent upon sufficient frequency coherence, which is notably present in bandwidth-efficient configurations (256 or 512 carriers in the 5-kHz experimental bandwidth). Using fewer carriers which are more widely spaced causes a loss

in frequency coherence (there is also an attendant loss in bandwidth efficiency), while using more carriers causes a loss in time coherence (ICI). Sensitivity to synchronization mismatch between the two transmitters, i.e., the delay difference in the time of their signal arrivals, was also investigated. The system was shown to tolerate delay differences typical of colocated transmitters (applications to cooperative MIMO scenarios with spatially separated transmitters would require scheduling). Interesting observations were also made by correlating the observed system performance to the environmental data, and in particular the wind speed. Future work will target the use of differentially coherent detection in the Alamouti MIMO framework.

REFERENCES

[1] B. Li, J. Huang, S. Zhou, K. Ball, M. Stojanovic, L. Freitag, and P. Willett, "MIMO-OFDM for high-rate underwater acoustic communications," *IEEE J. Ocean. Eng.*, vol. 34, no. 4, pp. 634–644, Oct. 2009.

[2] M. Stojanovic, "MIMO OFDM over underwater acoustic channels," in *Conf. Record 43rd Asilomar Conf. Signals Syst. Comput.*, Nov. 2009, pp. 605–609.

[3] B. Li and M. Stojanovic, "A simple design for joint channel estimation and data detection in an Alamouti OFDM system," in *Proc. OCEANS Conf.*, Sep. 2010, DOI: 10.1109/OCEANS.2010.5663867.

[4] M. Nordenvaad and T. Oberg, "Iterative reception for acoustic underwater MIMO communications," in *Proc. OCEANS Conf.*, 2006, DOI: 10.1109/OCEANS.2006.307060.

[5] S. Roy, T. Duman, V. McDonald, and J. Proakis, "High-rate communication for underwater acoustic channels using multiple transmitters and space time coding: Receiver structures and experimental results," *IEEE J. Ocean. Eng.*, vol. 32, no. 3, pp. 663–688, Jul. 2007.

[6] S. Roy, T. Duman, and V. McDonald, "Error rate improvement in underwater MIMO communications using sparse partial response equalization," *IEEE J. Ocean. Eng.*, vol. 34, no. 2, pp. 181–201, Apr. 2009.

[7] A. Rafati, H. Lou, and C. Xiao, "Soft-decision feedback turbo equalization for LDPC-coded MIMO underwater acoustic communications," *IEEE J. Ocean. Eng.*, vol. 39, no. 1, pp. 90–99, Jan. 2014.

[8] J. Zhang and Y. Zheng, "Frequency-domain turbo equalization with soft successive interference cancellation for single carrier MIMO underwater acoustic communications," *IEEE Trans. Wireless Commun.*, vol. 10, no. 9, pp. 2872–2882, Sep. 2011.

[9] J. Ling, X. Tan, T. Yardibi, J. Li, M. Nordenvaad, H. He, and K. Zhao, "On Bayesian channel estimation and FFT-based symbol detection in MIMO underwater acoustic communications," *IEEE J. Ocean. Eng.*, vol. 39, no. 1, pp. 59–73, Jan. 2014.

[10] S. Kaddouri, P.-P. Beaujean, P.-J. Bouvet, and G. Real, "Least square and trended Doppler estimation in fading channel for high-frequency underwater acoustic communications," *IEEE J. Ocean. Eng.*, vol. 39, no. 1, pp. 179–188, Jan. 2014.

[11] A. Song, M. Badiey, V. McDonald, and T. C. Yang, "Time reversal receivers for high data rate acoustic multiple-input multiple-output communication," *IEEE J. Ocean. Eng.*, vol. 36, no. 4, pp. 525–538, Oct. 2011.

[12] S. Alamouti, "A simple transmit diversity technique for wireless communications," *IEEE J. Sel. Areas Commun.*, vol. 16, no. 8, pp. 1451–1458, Oct. 1998.

[13] K. Lee and D. Williams, "A space-frequency transmitter diversity technique for OFDM systems," in *Proc. IEEE Global Telecommun. Conf.*, 2000, vol. 3, pp. 1473–1477.

[14] D.-B. Lin, P.-H. Chiang, and H.-J. Li, "Performance analysis of two-branch transmit diversity block-coded OFDM systems in time-varying multipath Rayleigh-fading channels," *IEEE Trans. Veh. Technol.*, vol. 54, no. 1, pp. 136–148, Jan. 2005.

[15] B. Li, S. Zhou, M. Stojanovic, L. Freitag, and P. Willett, "Multicarrier communication over underwater acoustic channels with nonuniform Doppler shifts," *IEEE J. Ocean. Eng.*, vol. 33, no. 2, pp. 198–209, Apr. 2008.

[16] K. Tu, T. Duman, M. Stojanovic, and J. Proakis, "Multiple-resampling receiver design for OFDM over Doppler-distorted underwater acoustic channels," *IEEE J. Ocean. Eng.*, vol. 38, no. 2, pp. 333–346, Apr. 2013.

[17] W. Li and J. Preisig, "Estimation of rapidly time-varying sparse channels," *IEEE J. Ocean. Eng.*, vol. 32, no. 4, pp. 927–939, Oct. 2007.

[18] Y. Kang, K. Kim, and H. Park, "Efficient DFT-based channel estimation for OFDM systems on multipath channels," *IET Commun.*, vol. 1, no. 2, pp. 197–202, Apr. 2007.

[19] J. Oliver, R. Aravind, and K. Prabhu, "Sparse channel estimation in OFDM systems by threshold-based pruning," *Electron. Lett.*, vol. 44, no. 13, pp. 830–832, 2008.

[20] C. Berger, S. Zhou, J. Preisig, and P. Willett, "Sparse channel estimation for multicarrier underwater acoustic communication: From subspace methods to compressed sensing," *IEEE Trans. Signal Process.*, vol. 58, no. 3, pp. 1708–1721, Mar. 2010.

[21] A. Radosevic, T. Duman, J. Proakis, and M. Stojanovic, "Selective decision directed channel estimation for UWA OFDM systems," in *Proc. 49th Annu. Allerton Conf. Commun. Control Comput.*, Sep. 2011, pp. 647–653.

[22] P. Qarabaqi and M. Stojanovic, "Statistical characterization and computationally efficient modeling of a class of underwater acoustic channels," *IEEE J. Ocean. Eng.*, vol. 38, Special Issue on Underwater Communications, no. 4, pp. 701–717, Oct. 2013.

[23] J. Kim, R. Heath, and E. Powers, "Receiver designs for Alamouti coded OFDM systems in fast fading channels," *IEEE Trans. Wireless Commun.*, vol. 4, no. 2, pp. 550–559, Mar. 2005.

[24] M. Krondorf and G. Fettweis, "Numerical performance evaluation for Alamouti space time coded OFDM under receiver impairments," *IEEE Trans. Wireless Commun.*, vol. 8, no. 3, pp. 1446–1455, Mar. 2009.

[25] L. Rugini, P. Banelli, H. Suraweera, and C. Yuen, "Performance of Alamouti space-time coded OFDM with carrier frequency offset," in *Proc. IEEE Global Telecommun. Conf.*, 2011, DOI: 10.1109/GLOCOM.2011.6133633.

Eduard Valera Zorita was born in Barcelona, Spain, in 1988. He received the B.Sc. and M.Sc. degrees in telecommunication engineering from the Universitat Politecnica de Catalunya (UPC), Barcelona, Spain, in 2012.

From September 2011 to March 2013, he was a Visiting Engineer in Signal Processing for Underwater Communications at Northeastern University, Boston, MA, USA, and the Massachusetts Institute of Technology, Cambridge, MA, USA. He is currently a Research Technician in Genome Architecture at the Centre for Genomic Regulation (CRG), Barcelona, Spain. His research interests include algorithm design, signal processing, wireless communications, and multiple-input–multiple-output (MIMO) systems.

Milica Stojanovic (SM'08–F'10) graduated from the University of Belgrade, Serbia, in 1988, and received the M.S. and Ph.D. degrees in electrical engineering from Northeastern University, Boston, MA, USA, in 1991 and 1993, respectively.

She was a Principal Scientist at the Massachusetts Institute of Technology (MIT), Cambridge, MA, USA, and in 2008, she joined Northeastern University where she is currently a Professor of Electrical and Computer Engineering. She is also a Guest Investigator at the Woods Hole Oceanographic Institution (WHOI), Woods Hole, MA, USA, and a Visiting Scientist at MIT. Her research interests include digital communications theory, statistical signal processing, and wireless networks, and their applications to underwater acoustic systems.

Dr. Stojanovic is an Associate Editor for the IEEE JOURNAL OF OCEANIC ENGINEERING and a past Associate Editor for the IEEE TRANSACTIONS ON SIGNAL PROCESSING and the IEEE TRANSACTIONS ON VEHICULAR TECHNOLOGY. She also serves on the Advisory Board of the IEEE Communication Letters, and chairs the IEEE Ocean Engineering Society's Technical Committee for Underwater Communication, Navigation, and Positioning.